The Astrophysical Journal, 871:196 (10pp), 2019 February 1 https://doi.org/10.3847/1538-4357/aaf869

Cosmological Tests of Gravity with the Latest Observations

Jian Li[1,2] and Gong-Bo Zhao[1,2,3]
[1] National Astronomical Observatories, Chinese Academy of Science, Beijing, 100101, People's Republic of China
[2] University of Chinese Academy of Sciences, Beijing, 100049, People's Republic of China
[3] Institute of Cosmology and Gravitation, University of Portsmouth, Portsmouth, PO1 3FX, UK
Received 2018 June 19; revised 2018 December 1; accepted 2018 December 11; published 2019 January 31

Abstract

We perform observational tests of modified gravity on cosmological scales following model-dependent and model-independent approaches using the latest astronomical observations, including measurements of the local Hubble constant, cosmic microwave background, the baryonic acoustic oscillations and redshift space distortions derived from galaxy surveys including the Sloan Digital Sky Survey BOSS and eBOSS, as well as the weak lensing observations performed by the CFHTLenS team. Combining all these data sets, we find a deviation from the prediction of general relativity in both the effective Newton's constant, $\mu(a, k)$, and in the gravitational slip, $\eta(a, k)$. The deviation is at a 3.1σ level in the joint $\{\mu(a, k), \eta(a, k)\}$ space using a two-parameter phenomenological model for μ and η, and reaches a 3.7σ level if a general parameterization is used. This signal, which may be subject to unknown observational systematics, or a sign of new physics, is worth further investigating with forthcoming observations.

Key words: cosmological parameters – cosmology: theory – dark energy – large-scale structure of universe

1. Introduction

The physical law governing the accelerating expansion of the universe, which was discovered by the redshift–luminosity relation revealed from supernovae observations (Riess et al. 1998; Perlmutter et al. 1999), remains unknown. In principle, the cosmic acceleration may suggest that approximately two-thirds of the total energy budget of the current universe is provided by an unknown energy component with a negative pressure, dubbed dark energy (DE; Copeland et al. 2006; Weinberg et al. 2013), or that we need a better understanding of the law of gravity.

The cosmological constant (CC) or the vacuum energy Λ, introduced by Einstein a century ago to prevent the universe from collapsing, has ironically become one of the most popular candidates of DE to give rise to the cosmic acceleration. Although the Λ-cold dark matter (ΛCDM) model can fit observations reasonably well, it suffers from severe theoretical issues (Weinberg 1989). Dynamical DE models (Copeland et al. 2006) can alleviate the cosmological constant problem to some extent, and phenomenological approaches in light of observations are actively being developed (see Zhao et al. 2017 for an example).

Nevertheless, general relativity (GR) is the most successful theory of gravity on scales from laboratory to the solar system. However, the validity of GR on cosmological scales is postulated, making it subject to scrutiny in theory, and to tests in observations. In fact, the expansion of the universe can accelerate without the existence of DE, if the left side of the Einstein equation gets modified. This essentially alters the response of the spacetime curvature to the energy-momentum distribution, and it is dubbed the modified gravity (MG) scenario (see Jain & Zhang 2008; Clifton et al. 2012; Joyce et al. 2015; Koyama 2016 for reviews on MG).

Both DE and modified gravity can yield the same expansion history of the universe after a required tuning of parameters; however, these two scenarios predict different growth histories for the cosmic structures. In other words, DE and MG can be degenerate at the background level, but this "dark degeneracy" can be broken at the perturbation level (Wang 2008).

Given our ignorance of the nature of DE and gravity, every possibility is worth exploring. In this regard, a combination of multiple cosmic probes, which is able to determine the cosmic expansion and structure growth history simultaneously, plays a key role for DE and MG studies.

In this work, we focus on observational tests of modified gravity scenarios on linear scales, on which the linear perturbation theory is valid. On these scales, MG can change the effective Newton's constant and/or the geodesics of photons (Koyama 2016), which leaves imprints on various kinds of cosmological observations, including the cosmic microwave background (CMB) and large-scale structure (LSS) of the universe. In particular, redshift space distortions (RSDs) (Kaiser 1987; Peacock et al. 2001) derived from the galaxy clustering of LSS spectroscopic surveys probe the change in the effective Newton's constant. Weak lensing (WL) measured from the imaging LSS surveys constrains the deviation of a photon's trajectory from the geodesic in a flat space, making RSD and WL highly complementary to each other for gravity tests (Zhao et al. 2010, 2012b; Song et al. 2011; Simpson et al. 2013; Planck Collaboration et al. 2016b).

In this analysis, we use the latest observations of CMB and LSS, combined with background cosmology probes, to derive constraints on modified gravity scenarios in a phenomenological way. Those background probes include the local measurement of the Hubble constant (H_0), the Hubble rate measurements using passive galaxies (OHD), and baryonic acoustic oscillations (BAOs; Peebles & Yu 1970; Eisenstein et al. 2005).

The paper is structured as follows. Section 2 describes the methodology used for this analysis, including the observational data sets, the rationale and framework of parameterizations of modified gravity, and details of the parameter estimation procedure. Our main results are presented in Section 3, followed by conclusions and discussions in Section 4.

2. Methodology

In this section, we present the methodology used for this analysis, including the general framework in which we parameterize the effect of modified gravity, data sets used, and details for parameter estimation.

2.1. General Framework of Parameterizing Modified Gravity

In this section, we discuss how we parameterize the universe in gravity models beyond GR. As we aim to use the growth of cosmic structure to break the dark degeneracy between MG and DE, in this work we assume a ΛCDM background cosmology, and parameterize the modification of gravity at the linear perturbation level.

In a flat Friedmann–Robertson–Walker universe, the metric in the conformal-Newtonian gauge reads

$$ds^2 = -a^2(\tau)[(1 + 2\Psi)d\tau^2 - (1 - 2\Phi)d\boldsymbol{x}^2], \quad (1)$$

where Φ and Ψ are functions depending on time (redshift z) and scale (wavenumber k). The energy-momentum conservation yields

$$\delta' + \frac{k}{aH}v - 3\Phi' = 0,$$
$$v' + v - \frac{k}{aH}\Psi = 0. \quad (2)$$

where δ refers to the density contrast, v represents the irrotational component of peculiar velocity, a and H are the scale factor and the Hubble rate, respectively, and the prime denotes derivatives with respect to $\ln a$.

In order to solve for $\{\delta, v, \Psi, \Phi\}$, two additional equations are required to close the system, and this is where a theory of gravity is required. Generically, the required equations are as follows (Zhao et al. 2009b; Pogosian et al. 2010):[4]

$$k^2\Psi = -4\pi G\rho a^2\mu(a, k)\Delta, \quad (3)$$

$$\frac{\Phi}{\Psi} = \eta(a, k), \quad (4)$$

where Equations (3) and (4) are called the modified Poisson equation and the gravitational slip equation, respectively. Δ, which is defined as $\delta + 3aHv/k$, denotes the gauge-invariant, comoving density contrast.

GR predicts that $\mu(a, k) = \eta(a, k) = 1$, and any deviation of these functions from unity, may be regarded as a smoking gun for modified gravity. Note that the $\mu(a, k)$ function can only be tested on sub-horizon scales, as it becomes irrelevant on super-horizon scales, on which only $\eta(a, k)$ can be tested observationally. On sub-horizon scales, both $\mu(a, k)$ and $\eta(a, k)$ have observational effects to be tested.

As Big Bang nucleosynthesis and CMB have been well explained with theories based on GR, we assume GR at high redshifts by setting $\mu(a, k) = \eta(a, k) = 1$ at $z > 50$, and test the deviation of μ and η from unity at lower redshifts.

Before introducing specific MG models to be tested, we parameterize our universe with the following set of cosmological parameters:

$$\boldsymbol{P} \equiv (\Omega_b h^2, \Omega_{cdm} h^2, \Theta_s, \tau, n_s, A_s, \mathcal{N}, \mathcal{X}), \quad (5)$$

where $\Omega_b h^2$ and $\Omega_{cdm} h^2$ denote the physical baryon and cold dark matter energy density, respectively; Θ_s is the ratio ($\times 100$) between the sound horizon and the angular diameter distance at the last scattering surface; τ is the re-ionization optical depth; and n_s and A_s denote the primordial power spectrum index and the amplitude of primordial power spectrum, respectively. In addition, $\mathcal{N}$ is used to denote several nuisance parameters that will be marginalized over when performing the likelihood analysis, and $\mathcal{X}$ denotes parameters to parameterize the $\mu(a, k)$ and $\eta(a, k)$ functions. As we only test gravity at the perturbation level, we assume a flat ΛCDM background cosmology.

2.2. Data Sets

The observational data sets used for this analysis include the CMB, supernovae (SNe), BAO and RSD, WL, galaxy power spectrum, and observational $H(z)$ data (OHD).

For CMB, we use the angular power spectra from the temperature and polarization maps provided by the Planck mission (Planck Collaboration et al. 2016a). The BAO-alone measurements we use include the isotropic BAO distance estimates using the 6dFGS (Beutler et al. 2011) and the Main Galaxy Sample of Sloan Digital Sky Survey Data Release (DR) 7 (Ross et al. 2015), and the anisotropic BAO measurement using the Lyα forest in BOSS DR11 (Delubac et al. 2015). For joint BAO and RSD, we use the following recent measurements:

- The consensus measurement at three effective redshifts of $z = \{0.38, 0.51, 0.61\}$ using the BOSS DR12 combined sample (Alam et al. 2017);
- The tomographic BAO and RSD measurement at nine effective redshifts in the range of $z \in [0.2, 0.75]$ derived from the same DR12 sample (Wang et al. 2018);[5] and
- The tomographic BAO and RSD measurement at four effective redshifts using the eBOSS (Dawson et al. 2016; Zhao et al. 2016) DR14 quasar sample based on the optimal redshift weighting method (Zhao et al. 2019).

Other observational data used for this analysis include the luminosity measurements from the joint light-curve analysis SNe sample (Betoule et al. 2014), the recent local H_0 measurement (Riess et al. 2016), the WL shear measurement from the CFHTLenS survey (Heymans et al. 2013), the galaxy power spectrum measurement from the WiggleZ redshift survey (Parkinson et al. 2012), and a compilation of $H(z)$ measurements using the ages of passive galaxies (Moresco et al. 2016).

To be explicit, we list these data sets and provide acronyms, meanings, and references in Table 1, and will use the acronyms shown in this table for later reference when presenting our results.

2.3. Parameter Estimation

Given a set of parameters in Equation (5), and the functional forms relating parameters $\mathcal{X}$ to the $\mu(a, k)$ and $\eta(a, k)$ functions,

[4] Alternative frameworks for parameterizing modified gravity have been proposed, e.g., Baker et al. (2013) and the effective field theory approach developed in Hu et al. (2014) and Raveri et al. (2014).

[5] Note that because (I) and (II) are derived from the same galaxy sample, we use them separately in our analysis.

Table 1
List of Data Sets Used for this Analysis, with Acronyms, Meanings, and References

Measurements	Meaning	References
PLC	CMB provided by the Planck collaboration	Planck Collaboration et al. (2016a)
6dF	BAO using the 6dFGS survey	Beutler et al. (2011)
MGS	BAO from the SDSS MGS sample	Ross et al. (2015)
LyαFB	BAO from the SDSS DR11 Lyα-forest sample	Delubac et al. (2015)
Alam	Consensus BAO + RSD using the BOSS DR12 combined sample	Alam et al. (2017)
Wang	Tomographic BAO + RSD using the BOSS DR12 combined sample	Wang et al. (2018)
eBOSS	Tomographic BAO + RSD using the eBOSS DR14 quasar sample	Zhao et al. (2019)
SNe	Luminosity from the JLA supernovae sample	Betoule et al. (2014)
H_0	Recent local H_0	Riess et al. (2016)
WL	Weak lensing shear using the CFHTLenS sample	Heymans et al. (2013)
$P(k)$	Power spectrum from WiggleZ	Parkinson et al. (2012)
OHD	$H(z)$ using the ages of passive galaxies	Moresco et al. (2016)
BAORSD	6dF+MGS+LyαFB+Wang	
BSH	BAORSD+SNe+H_0+OHD	
ALL17	PLC+BSH+WL+$P(k)$	
ALL18	ALL17+eBOSS	

Table 2
Mean and 68% CL Uncertainty for Parameters γ_L and σ_8 Derived from Four Data Combinations

	γ_L	σ_8
PLC+Alam	0.478 ± 0.029	0.835 ± 0.015
PLC+Wang	0.506 ± 0.032	0.818 ± 0.013
ALL17	0.509 ± 0.031	0.812 ± 0.013
ALL18	0.485 ± 0.031	0.828 ± 0.014

which will be introduced in Section 3, we use MGCAMB (Hojjati et al. 2011; Zhao et al. 2009b),[6] a variant of CAMB (Lewis et al. 2000)[7] working for modified gravity theories, to compute the observables, and use a modified version of CosmoMC (Lewis & Bridle 2002)[8] to sample the parameter space using the Monte Carlo Markov Chain method.

3. Results

We present our results in this section. To be clear, we present the "scale-independent" and "scale-dependent" cases separately, in which the μ and η functions depend on redshift z only, and on both redshift z and wavenumber k. For each case, we explicitly show the parameterization for the μ and η functions, before presenting the observational constraints. We also perform a principal component analysis (PCA) in both cases, to help interpret the result.

3.1. The Scale-independent Case

In this subsection, we consider MG scenarios in which the growth is scale-independent, i.e., μ and η are only functions of time, namely,

$$\mu = \mu(a);\ \eta = \eta(a). \tag{6}$$

We then parameterize the $\mu(a)$ and $\eta(a)$ functions using the gravitational growth index, power-law functions, and a more general parameterization based on piecewise constant bins in redshift.

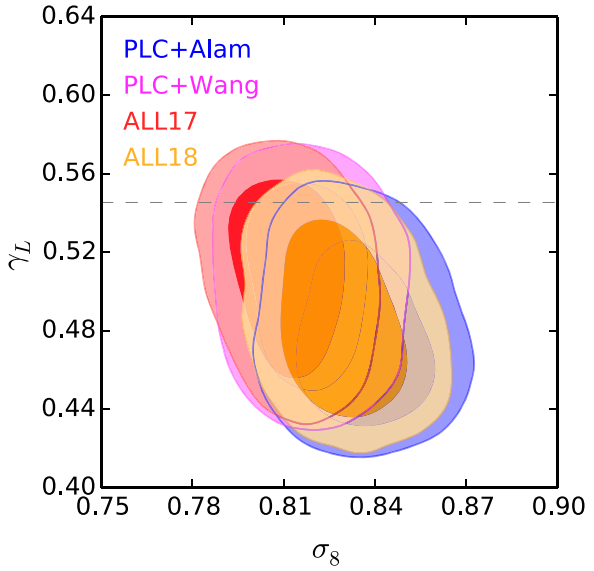

Figure 1. Contour plots for γ_L and σ_8 at the 68% and 95% confidence levels (CLs) derived from four data combinations as illustrated in the legend. The horizontal dashed line shows the GR value of $\gamma_L = 0.545$.

3.1.1. A Single-parameter Extension: The Gravitational Growth Index

As one of the minimal extensions to GR, the gravitational growth index γ_L (Linder 2005) has been widely used to search for signs of modified gravity phenomenologically (see Gil-Marín et al. 2018; Mueller et al. 2018; Wang et al. 2018; Zhao et al. 2019 for recent observational tests of gravity using γ_L). The gravitational growth index is defined as

$$f(a) \equiv \frac{d\log\delta}{d\log a} = \Omega_{\rm M}^{\gamma_L}(a), \tag{7}$$

[6] Available at http://aliojjati.github.io/MGCAMB/.
[7] Available at https://camb.info/.
[8] Available at https://cosmologist.info/cosmomc/.

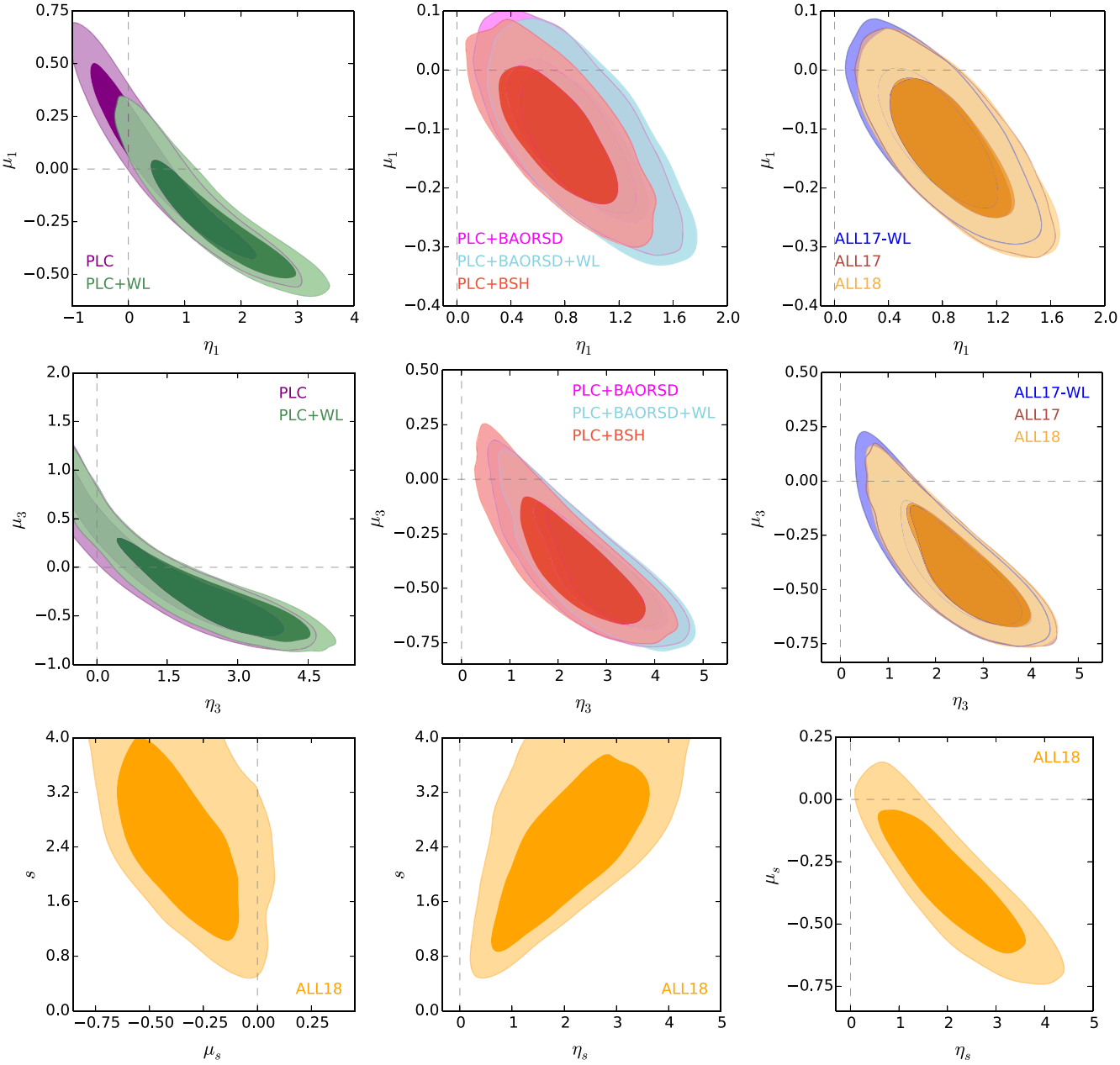

Figure 2. Upper and middle panels: the 68% and 95% contour plots for μ_s and η_s, where the upper panels are for the $s = 1$ and the middle panels are for $s = 3$. Contours for different data combinations are shown in separate panels to avoid confusion. Lower panels: 68% and 95% CL contour plots for μ_s and s (left) and for η_s and s (right) derived from ALL18. In all panels, the horizontal and vertical dashed lines denote $\mu_s = 0$ and $\eta_s = 0$, respectively, and the intersections of the dashed lines denote the GR model.

where $f(a)$ denotes the logarithmic growth rate as a function of scale factor a, δ is the matter overdensity, and $\Omega_{\rm M}(a)$ is the fractional energy density of matter at scale factor a.

In this framework (Pogosian et al. 2010),[9]

$$\mu(a) = \frac{2}{3}\Omega_{\rm M}^{\gamma_L - 1}\left[\Omega_{\rm M}^{\gamma_L} + 2 - 3\gamma_L + 3\left(\gamma_L - \frac{1}{2}\right)\Omega_{\rm M}\right]$$
$$\eta(a) = 1. \quad (8)$$

The joint constraints on γ_L and σ_8 (with all other parameters marginalized over) are shown in Table 2 and Figure 1 for four data combinations. As shown, the GR prediction of $\gamma_L = 0.545$ is generally consistent with the observations within the 95% CL.

3.1.2. A Three-parameter Extension: The Power-law Parameterization

A more general parameterization for $\mu(a)$ and $\eta(a)$ is to use power-law functions (Zhao et al. 2010):

$$\mu(a) = 1 + \mu_s a^s,$$
$$\eta(a) = 1 + \eta_s a^s. \quad (9)$$

We consider three cases where s is fixed to 1 (the linear model), 3 (the cubic model), or treated as a free parameter to be marginalized over.

[9] Here, we omit the variable a for $\Omega_{\rm M}$ for brevity. Also note that this formula is only valid for a constant γ_L in a ΛCDM background. For general cases, e.g., a time-dependent γ_L in a general cosmology, see Pogosian et al. (2010).

Table 3
Mean and 68% CL Uncertainties of the Power-law Model Parameters Derived from Different Data Combinations

	$s=1$		$s=3$	
	μ_1	η_1	μ_3	η_3
PLC	0.008 ± 0.280	0.642 ± 0.903	0.008 ± 0.538	1.465 ± 1.477
PLC+WL	-0.238 ± 0.194	1.546 ± 0.795	-0.197 ± 0.471	2.218 ± 1.428
PLC+BAORSD	-0.111 ± 0.083	0.855 ± 0.303	-0.404 ± 0.189	2.637 ± 0.857
PLC+BAORSD+WL	-0.128 ± 0.082	0.955 ± 0.301	-0.429 ± 0.175	2.858 ± 0.827
PLC+BSH	-0.110 ± 0.074	0.757 ± 0.277	-0.371 ± 0.195	2.298 ± 0.863
ALL17	-0.131 ± 0.075	0.863 ± 0.286	-0.405 ± 0.184	2.555 ± 0.835
ALL17-WL	-0.114 ± 0.074	0.773 ± 0.280	-0.376 ± 0.197	2.327 ± 0.847
ALL18	-0.132 ± 0.075	0.873 ± 0.289	-0.398 ± 0.184	2.516 ± 0.832

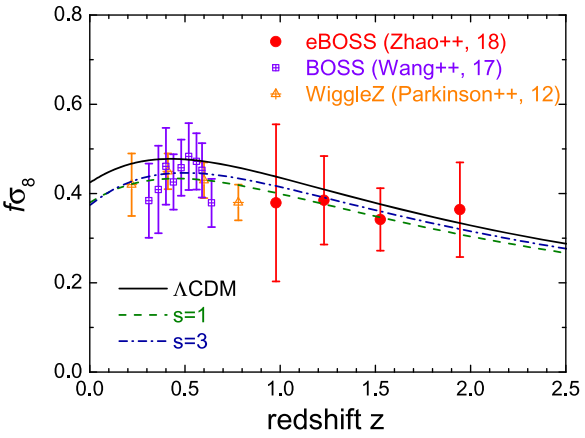

Figure 3. Best-fit $f\sigma_8$ of three gravity models including ΛCDM (black solid), a power law with $s = 1$ (green dashed), and a power law with $s = 3$ (blue dashed–dotted), overplotted with the observational data as illustrated in the legend.

We constrain the power-law model parameters using various data combinations, and show the results in Table 3 and Figure 2. As shown, the results for the cases of $s = 1$ and $s = 3$ are qualitatively similar, so we present both cases together. With PLC alone, GR is excluded at the 95% CL, and adding WL drags the contours toward a direction in which a large positive η_s and negative μ_s are favored (note that $\mu_s = \eta_s = 0$ for GR in our notation), which further excludes the GR model. With BAORSD, WL, SNe, and H_0 combined with PLC, the contours for both the $s = 1$ and $s = 3$ cases shrink significantly, and GR is excluded beyond the 95% CL level. Finally, combining all data, denoted as ALL18, yields the tightest constraint, which excludes the GR model at the 2.2σ and 3.1σ levels for the cases of $s = 1$ and $s = 3$, respectively.

Finally, we consider the general power-law models in which s is treated as a free parameter. We use the data set of ALL18 to constrain this model, and find that the constraints on μ_s and η_s get diluted compared with the cases of $s = 1$ or $s = 3$, due to marginalization over s, namely

$$\mu_s = -0.334 \pm 0.186;\ \eta_s = 2.090 \pm 0.904;\quad s = 2.474 \pm 0.770. \tag{10}$$

In this general case, GR is excluded at around the 2σ level.

Figure 3 shows the best-fit $f\sigma_8$ of the ΛCDM and power-law models, overplotted with observational data of RSD. As shown, models with a lower $f\sigma_8$, which means models predicting a weaker gravity, are favored by these recent RSD measurements.

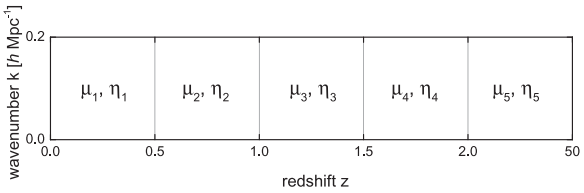

Figure 4. Illustration of the binning scheme in redshift z of the μ and η functions used in this work.

A similar analysis was performed by the Planck collaboration using slightly different power-law functions (Planck Collaboration et al. 2016b); their conclusion is consistent with ours, i.e., the deviation from GR can reach a 3σ level (depending on data combinations see Table 7 in Planck Collaboration et al. 2016b). As discussed therein, besides the RSD measurements, the signal is to some extent due to tensions within ΛCDM among data sets (see discussions in MacCrann et al. 2015; Di Valentino et al. 2016; Raveri 2016; Zhao et al. 2017 as well), which may suggest observational systematics, or new physics beyond ΛCDM.

3.1.3. The z-binning and PCA

In this section, we consider the most general parameterization for scale-independent μ and η functions using piecewise constant bins as free parameters. Given the sensitivity of current observations, we choose the redshift binning as illustrated in Figure 4,[10] thus we have 10 MG parameters in total.

We measure the μ and η bins using the ALL18 data set, and summarize the results in the left two columns of Table 4 and in panels (a), (b) of Figure 5. For a comparison with results using other parameterizations, we overplot a reconstruction of $\mu(z)$ and $\eta(z)$ with 68% CL uncertainty using the power-law parameterization shown in Equation (9) with the power index s marginalized over (the blue bands in Figure 5), which is in excellent agreement with our binned measurement.

As shown, most of the bins are consistent with the GR prediction, except for the μ bin at $1.0 < z < 1.5$ (i.e., μ_3 shown in Figure 4) and for the η bin at $0.5 < z < 1.0$ (i.e., η_2), both of which exhibit a deviation from GR at approximately the 1σ

[10] We assume GR outside the z and k ranges shown in Figure 4, i.e., $\mu = \eta = 1$ if $z > 50$ or $k > 0.2\ h^{-1}$ Mpc.

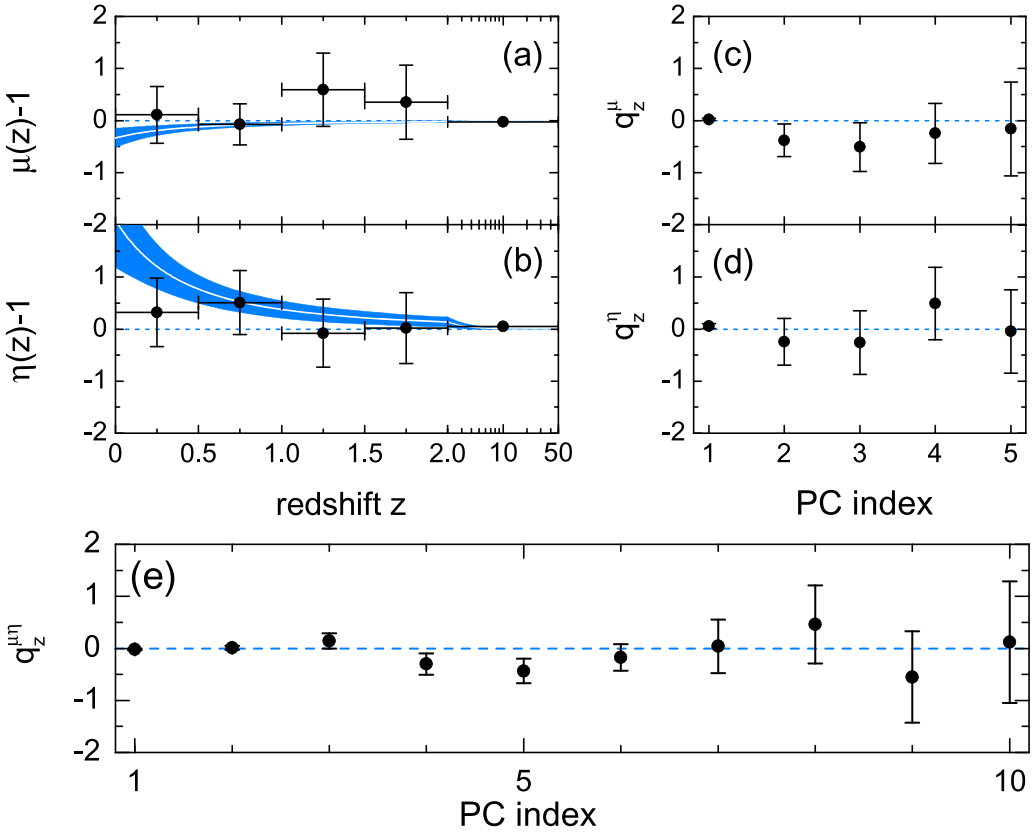

Figure 5. Constraints on scale-independent $\mu(z)$ and $\eta(z)$ functions and the associated PCA result derived from ALL18. Panels (a), (b): reconstructions of $\mu(z) - 1$ (panel a) and $\eta(z) - 1$ (panel (b)) using the redshift bins (data points with 68% CL error bars). The white curves and blue shaded bands show the mean and 68% uncertainty of $\mu(z) - 1$ and $\eta(z) - 1$ reconstructed using the power-law parameterization with s marginalized over. Panels (c), (d): mean and 68% CL uncertainties on coefficients of the principal components (PCs) of the μ or η functions with mutual marginalization (see the text for details). Panel (e): mean and 68% CL uncertainties on coefficients of the PCs of both μ and η functions.

Table 4
Mean and 68% CL Uncertainties on the $\mu_i - 1$ and $\eta_i - 1$ Bins (First Two Columns on the Left) and Associated PCA Results (the Remaining Four Columns)

$\mu_i - 1$	$\eta_i - 1$	q_z^{μ}	q_z^{η}	$q_z^{\mu\eta}$ (PC1-PC5)	$q_z^{\mu\eta}$ (PC6-PC10)
0.110 ± 0.546	0.320 ± 0.658	0.023 ± 0.021	0.059 ± 0.045	-0.021 ± 0.017	-0.175 ± 0.256
-0.074 ± 0.396	0.510 ± 0.613	-0.381 ± 0.314	-0.243 ± 0.449	0.013 ± 0.038	0.041 ± 0.515
0.590 ± 0.706	-0.080 ± 0.653	-0.507 ± 0.468	-0.258 ± 0.611	0.143 ± 0.147	0.459 ± 0.750
0.350 ± 0.711	0.020 ± 0.678	-0.246 ± 0.577	0.491 ± 0.693	-0.299 ± 0.204	-0.550 ± 0.879
-0.025 ± 0.036	0.050 ± 0.048	-0.161 ± 0.899	-0.045 ± 0.799	-0.436 ± 0.237	0.120 ± 1.170

level. However, as the errors are correlated with each other, it is difficult to interpret the result in a naïve way.

A natural way to interpret the correlated measurements is to perform a PCA to decorrelate the covariance matrix of the original parameters, which allows for the formation of a new set of parameters with a diagonal covariance matrix. The PCA method has been extensively used in cosmology, including implications in power spectrum measurements (Hamilton 2000; Hamilton & Tegmark 2000), DE equation of state (Huterer & Starkman 2003; Huterer & Cooray 2005; Crittenden et al. 2009; Zhao & Zhang 2010; Crittenden et al. 2012; Zhao et al. 2012a, 2017), and modified gravity parameters (Zhao et al. 2009a; Asaba et al. 2013; Hall et al. 2013; Hojjati et al. 2014, 2016).

The essence of the PCA is to diagonalize the covariance matrix $\boldsymbol{C_p}$ of the original correlated parameters denoted as $\boldsymbol{p}$,

$$\boldsymbol{C_p} = \boldsymbol{W^T} \Lambda \boldsymbol{W}, \tag{11}$$

where $\boldsymbol{W}$ is the decomposition matrix and $\boldsymbol{\Lambda}$ is the covariance matrix, which is diagonal, for the newly formed uncorrelated parameters $\boldsymbol{q} = \boldsymbol{Wp}$. The estimate of q with the associated uncertainty stored in $\boldsymbol{\Lambda}$ can identify which modes, i.e., uncorrelated linear combinations of the original parameters, deviate from the expected value given a theory, and how many modes can be constrained by data.

To investigate the consistency of the μ or η functions with unity, we first perform a PCA on the μ or η bins separately. The PCA result for the μ bins (with η bins marginalized over) and for the η bins (with μ bins marginalized over) are shown in the third and fourth columns and panels (c) and (d) of Figure 5. As shown, there are two modes, with principal component (PC) indices 2 and 3 shown in Figure 5, of μ deviating from the GR value, which is unity, at more than 1σ, while none of the η modes show deviation from GR given the uncertainty level. A χ^2 analysis using all the modes shows that the total signal-to-noise ratios

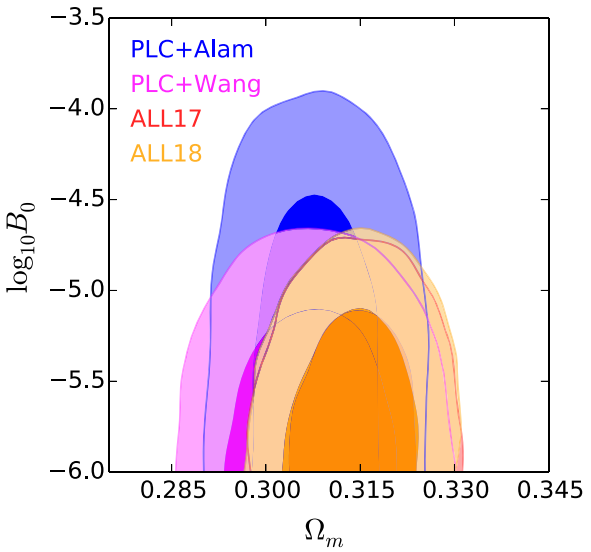

Figure 6. Contour plots for $\log_{10}B_0$ and Ω_m at the 68% and 95% CLs derived from four different data combinations illustrated in the legend.

Table 5
The 95% CL Upper Limit on $\log_{10}B_0$ Derived from Four Data Combinations

	$\log_{10}B_0$ (95% CL Upper Limit)
PLC+Alam	−4.276
PLC+Wang	−4.913
ALL17	−4.950
ALL18	−4.932

(S/Ns) of μ and η deviating from GR are 2.0σ and 1.6σ, respectively, based on the improvement in χ^2 only.

To quantify the deviation from GR without distinguishing between μ and η, we perform a PCA on the μ or η bins jointly, and show the result in the last two columns in Table 4 and in panel (e) of Figure 5. As illustrated, there are four joint μ and η modes, with PC indices 2, 3, 4, and 5, deviating from GR beyond the uncertainty level, which yields a 3.1σ signal in total.

The fact that using a large number of bins does not further improve the fitting compared with the power-law case means that the important features in the data can well be resolved by the power-law functions, which is consistent with what we show in panels (a), (b) in Figure 5. Actually, the PCA result conveys the same message: only 3 or 4 modes are needed to reproduce the total variance, which are essentially the degrees of freedom in the power-law functions.

3.2. The Scale-dependent Case

Now we consider more general cases in which the growth is scale-dependent, i.e., μ and η are functions of both scale and time, namely

$$\mu = \mu(k, a); \eta = \eta(k, a). \quad (12)$$

We then parameterize the $\mu(k, a)$ and $\eta(k, a)$ functions in the framework of the scalar-tensor theories, and use a more general parameterization based on pixelization in both scale and time.

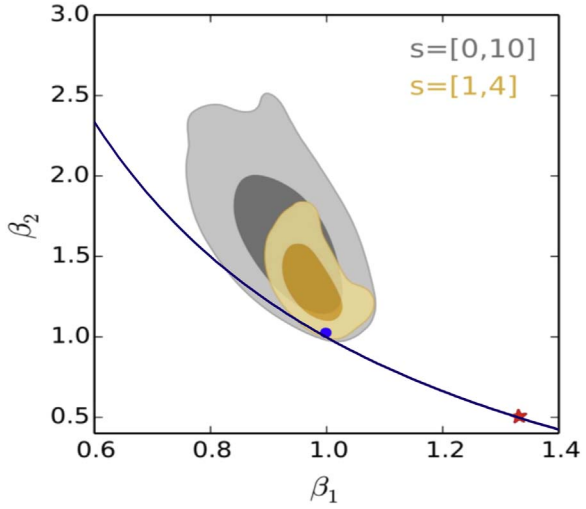

Figure 7. Contour plots for β_1 and β_2 the 68% and 95% CLs derived from ALL18 for two choices of flat priors applied on s. The blue solid curve shows the relation of $\beta_2 = 2/\beta_1 - 1$. The blue dot and the red star denote the ΛCDM and the $f(R)$ models, respectively.

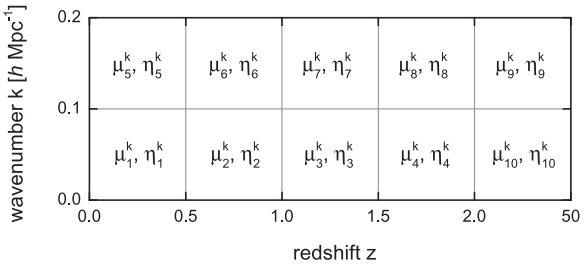

Figure 8. Illustration of the pixelization scheme in k and z of the μ and η functions used in this work.

Table 6
The Mean and 68% CL Uncertainty on β_1 and β_2 Derived from ALL18 with Two Different Flat Priors on s

Parameter	$s \in [1, 4]$	$s \in [0, 10]$
β_1	0.974 ± 0.033	0.928 ± 0.061
β_2	1.349 ± 0.165	1.647 ± 0.296

3.2.1. A Single-parameter Extension: The f(R) Model

The $f(R)$ theory (Bean et al. 2007; Hu & Sawicki 2007; Pogosian & Silvestri 2008; De Felice & Tsujikawa 2010) is a special case of the scalar-tensor theory with the following μ and η functions (Bertschinger & Zukin 2008):

$$\mu(a, k) = \frac{1 + \beta_1\lambda_1^2k^2a^s}{1 + \lambda_1^2k^2a^s},$$
$$\eta(a, k) = \frac{1 + \beta_2\lambda_2^2k^2a^s}{1 + \lambda_2^2k^2a^s}, \quad (13)$$

where β_1 and β_2 (denoting the coupling; dimensionless), s (the power index; dimensionless), and λ_1 and λ_2 (the length scales; in units of Mpc) are free parameters.

Table 7
The Mean and 68% CL Uncertainties on the Scale-dependent Functions of $\mu(k, z) - 1$ and $\eta(k, z) - 1$ (First Two Columns on the Left) and Associated PCA Results (the Remaining Four Columns)

$\mu_i^k - 1$	$\eta_i^k - 1$	q_{kz}^{μ}	q_{kz}^{η}	$q_{kz}^{\mu\eta}$ (PC1-PC10)	$q_{kz}^{\mu\eta}$ (PC11-PC20)
0.309 ± 0.768	-0.015 ± 0.594	-0.024 ± 0.023	0.036 ± 0.042	-0.017 ± 0.017	-1.212 ± 0.694
-0.177 ± 0.341	0.845 ± 0.656	-0.060 ± 0.199	-0.062 ± 0.324	-0.010 ± 0.038	-0.542 ± 0.740
0.696 ± 0.597	-0.297 ± 0.407	-0.282 ± 0.279	0.328 ± 0.479	0.201 ± 0.119	0.266 ± 0.799
0.175 ± 0.663	0.162 ± 0.701	-0.725 ± 0.400	0.227 ± 0.535	0.098 ± 0.153	-0.317 ± 0.901
-0.330 ± 0.910	-0.619 ± 0.762	0.631 ± 0.694	-0.779 ± 0.675	0.121 ± 0.172	0.409 ± 0.948
-0.679 ± 0.768	-0.700 ± 0.880	0.266 ± 0.762	-0.575 ± 0.757	-0.468 ± 0.243	-0.090 ± 0.970
-0.314 ± 0.971	-0.278 ± 1.072	0.003 ± 0.830	0.042 ± 0.767	0.054 ± 0.250	0.133 ± 1.001
-0.168 ± 1.105	-0.255 ± 1.019	0.349 ± 0.894	0.453 ± 0.885	-0.059 ± 0.437	0.102 ± 1.100
-0.013 ± 0.032	0.034 ± 0.043	0.373 ± 0.995	0.732 ± 1.039	-0.384 ± 0.476	0.645 ± 1.148
-0.035 ± 0.217	-0.001 ± 0.604	0.005 ± 1.060	-0.027 ± 1.116	-0.170 ± 0.557	0.407 ± 1.234

In $f(R)$,

$$\beta_1 = 4/3; \quad \beta_2 = 1/2; \quad \lambda_2^2/\lambda_1^2 = 4/3. \tag{14}$$

We fix $s = 4$ to closely mimic the ΛCDM model at the background level (Giannantonio et al. 2010), which leaves only one free parameter, λ_1, to be constrained. In practice, we vary $\log_{10}B_0$ together with other cosmological parameters where $B_0 \equiv 2H_0^2\lambda_1^2/c^2$. The Hubble constant H_0 and the speed of light c in the equation above make B_0 dimensionless, and $B_0 = 0$ corresponds to the ΛCDM limit.

The constraint on $f(R)$ gravity using four data sets is shown in Table 5 and Figure 6. First, we note that the constraint derived from PLC+Wang is much more stringent than that from PLC+Alam, which demonstrates the improvement on MG constraints using tomographic BAO and RSD measurements, as claimed in Zheng et al. (2019). Adding more data sets further improves the constraints, namely, the 95% CL upper limit of $\log_{10}B_0$ gets down to -4.93 using ALL18, which is tighter than a recent measurement, $\log_{10}B_0 < -4.54$, derived in Mueller et al. (2018). This is largely due to the additional information in the tomographic BAO and RSD measurements used for our analysis.

3.2.2. A Five-parameter Extension Motivated by the Scalar-tensor Model

The forms of μ and η for general scalar-tensor models are shown in Equation (13). Note that for scalar-tensor theories, the following consistency relation holds (Zhao et al. 2009b; Hojjati et al. 2011):

$$\beta_1 = \frac{\lambda_1^2}{\lambda_2^2}; \quad \beta_2 = \frac{2}{\beta_1} - 1. \tag{15}$$

However these relations are not applied as a constraint in our analysis, but used for a direct comparison with our observational constraint.

It is worth noting that a large s can make other parameters trivial in the joint parameter estimation, thus a prior on s is needed. In this work, we make two choices of the flat prior for s. One is motivated by scalar-tensor theories, which is $s \in [1, 4]$ (Zhao et al. 2009b; Giannantonio et al. 2010), with another one being more conservative, namely $s \in [0, 10]$.

We show the constraints of β_1 and β_2 derived from ALL18 with all other parameters marginalized over in Figure 7 and Table 6. As shown in both cases, GR ($\beta_1 = \beta_2 = 1$) is consistent with data at the 68% CL, and the scalar-tensor theory prediction, Equation (15), is allowed within the 68% CL uncertainty. However, the $f(R)$ model discussed in Section 3.2.1 with $\beta_1 = 4/3$, $\beta_2 = 1/2$ is strongly disfavored by data. This is understandable, as we have seen from the power-law case in Section 3.1.2 (see Figure 3) that data favor a weaker gravity, while in $f(R)$, gravity is always stronger than that in GR.

3.2.3. The k, z-pixelization and PCA

We parameterize the functions of μ and η using pixels in the (k, z) plane as illustrated in Figure 8, constrain the pixels using the ALL18 data set, and present the results in Table 7 and Figure 9 in a similar way as we did for the k-independent case in Section 3.1.3.

Looking at the constraints on the pixels shown in the left two columns in Table 7 and in panels (a), (b) in Figure 9, we find that pixels μ_3^k, η_2^k, and η_6^k, as denoted in Figure 8, show a deviation from GR at more than the 1σ level, and interestingly, the η function at $z \in [0.5, 1.0]$ shows a signal of scale-dependence at around the 2σ level.

A PCA on the μ and η pixels with the other parameters marginalized over shows that there are three (two) μ (η) modes deviating from GR beyond the uncertainty, which corresponds to 2.6σ and 2.0σ signals, respectively. A PCA on all the μ and η pixels jointly reveals four modes, with PC indices 3, 5, 6, and 11 deviating from GR noticeably, making a total signal at the level of 3.7σ. This means that only a small number of degrees of freedom is required to capture the feature in the data, which is consistent with the scale-independent case.

4. Conclusion and Discussion

Theoretical and observational approaches are being developed in order to test the validity of postulating GR on cosmological scales, which is a significant extrapolation of our knowledge of gravity from scales within the solar system. Observational tests of theoretical models thus play a crucial role in the search for the ultimate theory of gravity governing the observed cosmic acceleration. As a large number of modified gravity theories have been proposed (see reviews of Jain & Zhang 2008; Clifton et al. 2012; Joyce et al. 2015; Koyama 2016), it is efficient to perform observational gravity tests following a phenomenological approach.

In this work, we parameterize the effect of modified gravity using two functions μ and η on linear scales, which are generically dependent on both time and scale, describing the effective Newton's constant and the gravitational slip,

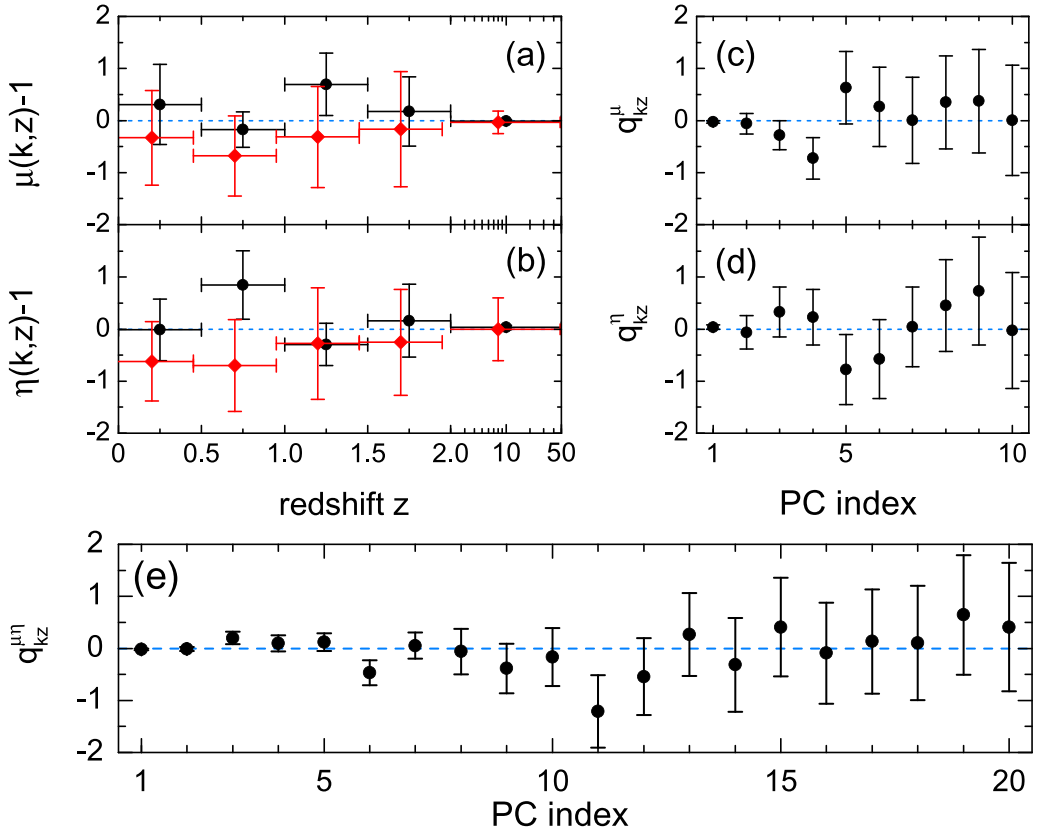

Figure 9. Constraints on scale-dependent $\mu(k, z)$ and $\eta(k, z)$ functions and the associated PCA results derived from ALL18. Panels (a), (b): reconstructions of $\mu(k, z) - 1$ (panel (a)) and $\eta(k, z) - 1$ (panel b) using the z and k pixels (data points with 68% CL error bars). The black circles with error bars and red diamonds with error bars represent pixels within $k \in [0, 0.1]$ and $k \in [0.1, 0.2]$, respectively. Panels (c), (d): the mean and 68% CL uncertainties on coefficients of the PCs of the μ or η functions with mutual marginalization. Panel (e): the mean and 68% CL uncertainties on coefficients of the principal components (PCs) of both μ and η functions.

Table 8
The Improved χ^2 ($\Delta\chi^2$), the S/N Calculated Using the Improved χ^2 Alone (SNR $\equiv \sqrt{|\Delta\chi^2|}$), the Additional Parameters to the ΛCDM Model (ΔN_p), and the S/N per the Additional Parameter (SNR/ΔN_p) for the Constraint on MG Models Studied in this Work Using the ALL18 Data Set

Model	$\Delta\chi^2$	SNR	ΔN_p	SNR/ΔN_p
ΛCDM	0	0	0	...
γ_L	−4.8	2.2	1	2.2
Power law, $s = 1$	−12.4	3.5	2	1.7
Power law, $s = 3$	−12.8	3.6	2	1.8
Power law, s floating	−12.4	3.5	3	1.2
BZ model, $s \in [0, 10]$	−11.2	3.3	5	0.66
BZ model, $s \in [1, 4]$	−12.2	3.5	5	0.7
z-binning	−10.6	3.3	10	0.33
k, z-pixelization	−17.0	4.1	20	0.21

respectively, and use the latest observational data to constrain parameters for these two functions.

By assuming that μ and η only depend on time to start with, we further parameterize them using the gravitational growth index γ_L, power-law functions and piecewise constant bins progressively. We find no signal of modified gravity from current observations using γ_L, which is a one-parameter extension of ΛCDM, but see a significant deviation from GR (at around the 3σ level) using the power-law parameterization (a two-parameter extension). Using a more general parameterization with piecewise constants in redshifts (a ten-parameter extension), we find that the significance stays at the same level, signaling that the important features in the data, which can be described by a scale-independent growth, can well be extracted using power-law functions for μ and η.

We then further explore more general cases in which both μ and η depend on time and scale. We parameterize these two functions in frameworks of $f(R)$ gravity (a one-parameter extension of GR), scalar-tensor theory (a five-parameter extension), and using pixels (a twenty-parameter extension). We find no significant deviation from GR in $f(R)$ or in the scalar-tensor models, but a deviation at a 3.7σ level is revealed when using pixels. We caution that the S/N quoted here is computed using the improved χ^2 of the fitting, thus is not sufficient for a model selection. In Table 8, we show the improvement in the χ^2, as well as that normalized by the number of additional parameters, for the MG models. As shown, the most "parameter-economic" model, in which SNR/ΔN_p get maximized, is the γ_L model, which shows no deviation from GR. The power-law models with $s = 1$ and $s = 3$ are slightly less parameter-economic, but a significant deviation from GR is seen in such models. An evaluation of the Bayesian evidence is needed for a formal model selection, which is left for a future work.

The signal we find in this work is to some extent due to tensions among data sets on cosmological scales within the ΛCDM model, which have been investigated by the community. This could be due to contaminations from unknown systematics in the observations, or a sign of new physics, which can be further studied by complementary GR tests on nonlinear scales (Zhang et al. 2007; Reyes et al. 2010; Cabré et al. 2012;

Jain et al. 2013; Vikram et al. 2013, 2018; Berti et al. 2015; Wilcox et al. 2015; Liu et al. 2016; Fang et al. 2017; Falck et al. 2018). Forthcoming large astronomical surveys, including the Dark Energy Spectroscopic Instrument (DESI Collaboration et al. 2016), Prime Focus Spectrograph (Takada et al. 2014), and *Euclid* (Amendola et al. 2018), will provide rich observational data for GR tests across a large range of scales.

We thank Yuting Wang, Xiao-Dong Li, Eva-Maria Mueller, and Will Percival for discussions. This work is supported by the National Key Basic Research and Development Program of China (No. 2018YFA0404503), and by NSFC Grants 11720101004, 11673025 and 11711530207. This research used the resources of the SCIAMA cluster supported by University of Portsmouth.

ORCID iDs

Gong-Bo Zhao https://orcid.org/0000-0003-4726-6714

References

Alam, S., Ata, M., Bailey, S., et al. 2017, MNRAS, 470, 2617
Amendola, L., Appleby, S., Avgoustidis, A., et al. 2018, LRR, 21, 2
Asaba, S., Hikage, C., Koyama, K., et al. 2013, JCAP, 8, 29
Baker, T., Ferreira, P. G., & Skordis, C. 2013, PhRvD, 87, 024015
Bean, R., Bernat, D., Pogosian, L., Silvestri, A., & Trodden, M. 2007, PhRvD, 75, 064020
Berti, E., Barausse, E., Cardoso, V., et al. 2015, CQGra, 32, 243001
Bertschinger, E., & Zukin, P. 2008, PhRvD, 78, 024015
Betoule, M., Kessler, R., Guy, J., et al. 2014, A&A, 568, A22
Beutler, F., Blake, C., Colless, M., et al. 2011, MNRAS, 416, 3017
Cabré, A., Vikram, V., Zhao, G.-B., Jain, B., & Koyama, K. 2012, JCAP, 7, 034
Clifton, T., Ferreira, P. G., Padilla, A., & Skordis, C. 2012, PhR, 513, 1
Copeland, E. J., Sami, M., & Tsujikawa, S. 2006, IJMPD, 15, 1753
Crittenden, R. G., Pogosian, L., & Zhao, G.-B. 2009, JCAP, 12, 025
Crittenden, R. G., Zhao, G.-B., Pogosian, L., Samushia, L., & Zhang, X. 2012, JCAP, 2, 048
Dawson, K. S., Kneib, J.-P., Percival, W. J., et al. 2016, AJ, 151, 44
De Felice, A., & Tsujikawa, S. 2010, LRR, 13, 3
Delubac, T., Bautista, J. E., Busca, N. G., et al. 2015, A&A, 574, A59
DESI Collaboration, Aghamousa, A., Aguilar, J., et al. 2016, arXiv:1611.00036
Di Valentino, E., Melchiorri, A., & Silk, J. 2016, PhRvD, 93, 023513
Eisenstein, D. J., Zehavi, I., Hogg, D. W., et al. 2005, ApJ, 633, 560
Falck, B., Koyama, K., Zhao, G.-B., & Cautun, M. 2018, MNRAS, 475, 3262
Fang, W., Li, B., & Zhao, G.-B. 2017, PhRvL, 118, 181301
Giannantonio, T., Martinelli, M., Silvestri, A., & Melchiorri, A. 2010, JCAP, 4, 030
Gil-Marín, H., Guy, J., Zarrouk, P., et al. 2018, MNRAS, 477, 1604
Hall, A., Bonvin, C., & Challinor, A. 2013, PhRvD, 87, 064026
Hamilton, A. J. S. 2000, MNRAS, 312, 257
Hamilton, A. J. S., & Tegmark, M. 2000, MNRAS, 312, 285
Heymans, C., Grocutt, E., Heavens, A., et al. 2013, MNRAS, 432, 2433
Hojjati, A., Plahn, A., Zucca, A., et al. 2016, PhRvD, 93, 043531
Hojjati, A., Pogosian, L., Silvestri, A., & Zhao, G.-B. 2014, PhRvD, 89, 083505
Hojjati, A., Pogosian, L., & Zhao, G.-B. 2011, JCAP, 8, 5
Hu, B., Raveri, M., Frusciante, N., & Silvestri, A. 2014, PhRvD, 89, 103530
Hu, W., & Sawicki, I. 2007, PhRvD, 76, 064004
Huterer, D., & Cooray, A. 2005, PhRvD, 71, 023506
Huterer, D., & Starkman, G. 2003, PhRvL, 90, 031301
Jain, B., Vikram, V., & Sakstein, J. 2013, ApJ, 779, 39
Jain, B., & Zhang, P. 2008, PhRvD, 78, 063503
Joyce, A., Jain, B., Khoury, J., & Trodden, M. 2015, PhR, 568, 1
Kaiser, N. 1987, MNRAS, 227, 1
Koyama, K. 2016, RPPh, 79, 046902
Lewis, A., & Bridle, S. 2002, PhRvD, 66, 103511
Lewis, A., Challinor, A., & Lasenby, A. 2000, ApJ, 538, 473
Linder, E. V. 2005, PhRvD, 72, 043529
Liu, X., Li, B., Zhao, G.-B., et al. 2016, PhRvL, 117, 051101
MacCrann, N., Zuntz, J., Bridle, S., Jain, B., & Becker, M. R. 2015, MNRAS, 451, 2877
Moresco, M., Pozzetti, L., Cimatti, A., et al. 2016, JCAP, 5, 014
Mueller, E.-M., Percival, W., Linder, E., et al. 2018, MNRAS, 475, 2122
Parkinson, D., Riemer-Sørensen, S., Blake, C., et al. 2012, PhRvD, 86, 103518
Peacock, J. A., Cole, S., Norberg, P., et al. 2001, Natur, 410, 169
Peebles, P. J. E., & Yu, J. T. 1970, ApJ, 162, 815
Perlmutter, S., Aldering, G., Goldhaber, G., et al. 1999, ApJ, 517, 565
Planck Collaboration, Ade, P. A. R., Aghanim, N., et al. 2016a, A&A, 594, A13
Planck Collaboration, Ade, P. A. R., Aghanim, N., et al. 2016b, A&A, 594, A14
Pogosian, L., & Silvestri, A. 2008, PhRvD, 77, 023503
Pogosian, L., Silvestri, A., Koyama, K., & Zhao, G.-B. 2010, PhRvD, 81, 104023
Raveri, M. 2016, PhRvD, 93, 043522
Raveri, M., Hu, B., Frusciante, N., & Silvestri, A. 2014, PhRvD, 90 043513
Reyes, R., Mandelbaum, R., Seljak, U., et al. 2010, Natur, 464, 256
Riess, A. G., Filippenko, A. V., Challis, P., et al. 1998, AJ, 116, 1009
Riess, A. G., Macri, L. M., Hoffmann, S. L., et al. 2016, ApJ, 826, 56
Ross, A. J., Samushia, L., Howlett, C., et al. 2015, MNRAS, 449, 835
Simpson, F., Heymans, C., Parkinson, D., et al. 2013, MNRAS, 429, 2249
Song, Y.-S., Zhao, G.-B., Bacon, D., et al. 2011, PhRvD, 84, 083523
Takada, M., Ellis, R. S., Chiba, M., et al. 2014, PASJ, 66, R1
Vikram, V., Cabré, A., Jain, B., & VanderPlas, J. T. 2013, JCAP, 8, 020
Vikram, V., Sakstein, J., Davis, C., & Neil, A. 2018, PhRvD, 97, 104055
Wang, Y. 2008, JCAP, 5, 021
Wang, Y., Zhao, G.-B., Chuang, C.-H., et al. 2018, MNRAS, 481, 3160
Weinberg, D. H., Mortonson, M. J., Eisenstein, D. J., et al. 2013, PhR, 530, 87
Weinberg, S. 1989, RvMP, 61, 1
Wilcox, H., Bacon, D., Nichol, R. C., et al. 2015, MNRAS, 452, 1171
Zhang, P., Liguori, M., Bean, R., & Dodelson, S. 2007, PhRvL, 99, 141302
Zhao, G.-B., Crittenden, R. G., Pogosian, L., & Zhang, X. 2012a, PhRvL, 109, 171301
Zhao, G.-B., Giannantonio, T., Pogosian, L., et al. 2010, PhRvD, 81, 103510
Zhao, G.-B., Li, H., Linder, E. V., et al. 2012b, PhRvD, 85, 123546
Zhao, G.-B., Pogosian, L., Silvestri, A., & Zylberberg, J. 2009a, PhRvL, 103, 241301
Zhao, G.-B., Pogosian, L., Silvestri, A., & Zylberberg, J. 2009b, PhRvD, 79, 083513
Zhao, G.-B., Raveri, M., Pogosian, L., et al. 2017, NatAs, 1, 627
Zhao, G.-B., Wang, Y., Ross, A. J., et al. 2016, MNRAS, 457, 2377
Zhao, G.-B., Wang, Y., Saito, S., et al. 2019, MNRAS, 482, 3497
Zhao, G.-B., & Zhang, X. 2010, PhRvD, 81, 043518
Zheng, J., Zhao, G.-B., Li, J., et al. 2019, MNRAS, 484, 442